

www.acsami.org Research Article

Non-Covalent Coatings on Carbon Nanotubes Mediate Photosensitizer Interactions

Christopher P. Horoszko, Peter J. Schnatz, Januka Budhathoki-Uprety, Rahul V. Rao-Pothuraju, Ronald L. Koder, and Daniel A. Heller*



Cite This: ACS Appl. Mater. Interfaces 2021, 13, 51343-51350



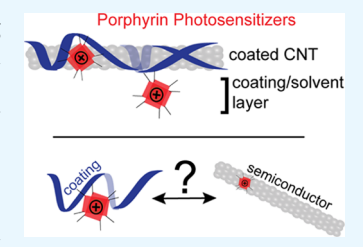
ACCESS

Metrics & More

Article Recommendations

Supporting Information

ABSTRACT: Carbon nanotube-based donor-acceptor devices are used in applications ranging from photovoltaics and sensors to environmental remediation. Non-covalent contacts between donor dyes and nanotubes are often used to optimize sensitization and scalability. However, inconsistency is often observed despite donor dye studies reporting strong donor—acceptor interactions. Here, we demonstrate that the dye binding location is an important factor in this process: we used coated-acceptor chromatic responses and find that dye binding is affected by the coating layer. The emission response to free- and protein-sequestered porphyrin was tested to compare direct and indirect dye contact. An acceptor complex that preferentially red-shifts in response to sequestered porphyrin was identified. We observe inconsistent optical signals that



suggest porphyrin-dye interactions are best described as coating-centric; therefore, the coating interface must be considered in application and assay design.

KEYWORDS: donor-acceptor, binding, metrology, interface, hybrid, dyes, substrate

■ INTRODUCTION

Semiconducting single-walled carbon nanotubes (SWCNTs) exhibit high efficiency charge separation and large carrier mobilities optimal for applications such as photovoltaics and sensors. The near-ballistic charge-transport properties of nanotubes¹ led to the use of non-covalent surface modifications based on the idea that these coatings do not interrupt the π -system of the material. However, spectroscopic evidence of non-linear excited-state processes² might indicate that excitonic processes are influenced by the surface coating.^{3–5} Due to the relationship between the SWCNT excited state and coatings, donor dyes may not be interacting, as is commonly assumed, with the π -system of the sidewall.^{3,4,6,7} Donor—acceptor spectroscopy used to evaluate surface interactions may thus be complicated by interactions of a dye both with the nanotube sidewall and its coating.

SWCNT-coating polymers (both conducting and non-conducting types) are thought to act as binding agents that increase sensitizer (donor) density on the SWCNT (acceptor) substrate. Guanine (G)-rich ssDNA, for example, is a relatively efficient photoconversion polymer on SWCNTs.⁸ Strong coupling between porphyrin and carbon nanotubes (likely the coating interface) has been inferred because the porphyrin absorption/emission response in complexes with ssDNA is qualitatively similar to the response in complex with ssDNA-coated SWCNTs.⁸ For example, in this same study, an illuminated donor—acceptor substrate resulted in a photocurrent efficiency of only around 1.5%. Considering that porphyrins couple electronically to (G)-containing ssDNA,⁹ which should promote good sensitizing interactions, it is

possible that the coating itself is an important factor in application efficiency if binding occurs over more than the assumed CNT sidewall.

Spectroscopic studies of donor—acceptor systems have shown that increases in π – π hybridization between donor—acceptor systems result in both red-shifts and intensity loss of the porphyrin Soret absorbance and Q-band emission. 8,10–18 Likewise, several studies report spectroscopic signatures that benchmark proximity to the SWCNT sidewall. In one example, the presence of a strong electric dipole (separated charge) introduced into the SWCNT coating produced a large SWCNT absorbance/emission red-shift. 19–21 In the second example, the SWCNT π -plasmon absorbance in the ultraviolet (UV) region was used to detect a possible surface redox phenomenon. To distinguish optical responses from porphyrin that is free, or not free, to bind the SWCNT, we note that the curved nanotube surface barely interacts with molecules, such as proteins, that are similar to or greater in size than the tube diameter. 23,24

In this work, we examined the SWCNT-porphyrin hybrid system from the perspective of the nanotube acceptor to ask whether non-covalent functionalization impacts binding assessment. To test the role of the acceptor chromatic shift on direct

Received: July 27, 2021 Accepted: October 7, 2021 Published: October 21, 2021





binding interactions, we used a library of coatings to screen porphyrins, either freely interacting or sequestered by a binding protein. A coating was identified that mediated significant yet opposite acceptor optical response to indirectly interacting porphyrins. To determine the influence of the coating in this acceptor complex, we spectroscopically evaluated porphyrin interactions with the coatings alone or with the coated-acceptor complex. Our findings necessitate an update from the current SWCNT interfacial interaction model to one that considers both observed coating-nanotube hybridization effects and dye sensitization inefficiency.

EXPERIMENTAL SECTION

Reagents and Material Preparation. Helically dispersing polycarbodiimide polymers were synthesized as previously described.²⁵ Synthesized polymers were washed with diethyl ether (Acros 61508-0010) three times and then evaporated. Raw polycarbodiimide was suspended in water with mild bath sonication. Other encapsulations used in this work were ssDNA (IDT, customordered $(GT)_{15/30}$ and $(AT)_{15/30}$, standard desalting), carboxymethyl cellulose sodium salt (CMC) (Sigma C4888), sodium deoxycholate (SDC) (Sigma D6750), and PEG-cera(mide) (Avanti 880680). HiPco (Unidym) nanotubes (initial library) or CoMoCat nanotubes (Sigma 775533) containing the (6,5), (8,3), and (7,5) chiralities were suspended after mixing 1 mg of CoMoCat with 1 mL of aqueous encapsulation (10 mg/mL) in deionized water (18.2 M Ω). This mixture was probe tip-sonicated (Sonics & Materials, Sonics Vibracell VCX750) for 30 min with 10 W using a 3 mm stepped microtip probe (Sonics and Materials 422-17) immersed in a 2 mL Eppendorf in a -20 °C cold block (Biocision CoolRack M30). The resulting black suspension was centrifuged for 10 min at 30,000 rcf (Eppendorf Centrifuge 5430R). The top 90% of this suspension was collected and then ultracentrifuged for 30 min at 171,180 rcf (Sorvall Discovery 90SE). The top 80% of the resulting supernatant was collected into a new Eppendorf and positioned on top of a Neodymium magnet (Applied Magnets) for 3 days to clear residual metal particles. After 3 days, the supernatant above the fuzzy/loose pellet was collected and stored at 4 °C with 0.05% w/v sodium azide. All coatings produced good yields (>30 mg/L) indicating efficient and stable complexation. A working nanotube suspension was prepared using three wash-spin cycles with deionized water in a centrifugal filter (Millipore Amicon, 100 kDa MWCO) followed by a final resuspension with a desired volume of deionized water and final bench centrifugation for 10 min at 30,000 rcf. Aqueous buffer reported in this work consisted of a 100 mM borate solution at pH 9 (Thermo 28341) containing 100 mM sodium chloride (Fisher S2711). Sieve-dried DMSO (Fisher D1281) was used to dissolve the following porphyrin dyes: protoporphyrin IX, PP (Frontier Scientific P5629), 5,10,15,20-tetraphenyl-21H,23Hporphine, TPP (Sigma 160997), protoporphyrin IX iron(III), hemin (Sigma 51280), 5,10,15,20-tetraphenyl-21H,23H-porphine iron(III) chloride, TPPF (Sigma 259071), iron(III) mono(4-sulfonatophenyl)triphenyl porphine chloride, MSTPF (Frontier M14841), 2,3,7,8,12,13,17,18-octaethyl-21H,23H-porphine, OEP (Sigma 252409), 2,3,7,8,12,13,17,18-octaethyl-21H,23H-porphine iron(III) chloride, OEPF (Sigma 257532), and iron(III) isohematoporphyrin IX chloride, IHPF (Frontier I40055). Porphyrin stock solutions were prepared in DMSO to 800 μM or 1.5 mM. A non-ionic surfactant, IGEPAL CA-630 (Sigma I8896), was used at 0.05% v/v. PCD-446 stock solution was prepared by dissolving 3 mg of the solid in 1 mL of borate buffer: the molecular weight of the 446 monomer was 285 Da, with a degree of polymerization at approximately 30, making 446 approximately 8500 Da. Mixed diameter SWCNTs adsorb 5-10 coating polymers per tube. ABTS was received as a ready-to-use solution containing hydrogen peroxide (Sigma 11684302001). The half-life of the ABTS cation radical is short in alkaline media, and its absorbance max is therefore red-shifted with respect to the manufacturer conditions (405 nm shifted to roughly 430 nm).

Binding Protein Expression and Purification. The negatively supercharged artificial hemin binding protein H4(-28)²⁶ was expressed in BL21(DE3) *Escherichia coli* expression strains using genes subcloned into pET32 expression plasmids (Novagen 69015) and purified using methods published previously.²⁷ Porphyrin complex formation was performed using six equimolar additions with 10 min incubation periods between additions,²⁸ and complexes were isolated using PD-10 desalting columns (GE Life Sciences 17085101).

UV-Vis-NIR Steady-State Spectrophotometry. Spectrophotometric measurements were carried out with a Jasco V-670 instrument (Jasco, Inc.) containing a halogen/deuterium lamp and 1 cm path-length quartz cuvettes (Starna 16.40-Q-10/Z15). The extinction coefficient used to calculate concentrations of non-ssDNA-SWCNT was $\varepsilon(630 \text{ nm}) = 0.036 \text{ L·mg}^{-1} \cdot \text{cm}^{-1}$ for HiPco suspensions or ε (910 nm) = 0.02083 L·mg⁻¹·cm⁻¹ for CoMoCat suspensions. For ssDNA-SWCNT, the extinction coefficient was $\varepsilon(910 \text{ nm}) = 0.02083$ $L \cdot mg^{-1} \cdot cm^{-1}$ for CoMoCat suspensions or $\varepsilon(910 \text{ nm}) = 0.02254 \text{ L} \cdot$ mg⁻¹·cm⁻¹ for HiPco suspensions. For ABTS assays, cuvettes were blanked first with solvent and coating/porphyrin. A 1:1 dilution of the ABTS reagent was added to the measurement cuvette, and the contents were mixed by pipette for 10 s. All spectrophotometer measurements used a data interval of 0.5 nm, UV-vis bandwidth of 2 nm, NIR bandwidth of 8 nm, medium response time, 1000 nm/min scan speed, 10 mm cell path length, and a stepped filter exchange.

Nanotube Photoluminescence Spectroscopy. Well-plate photoluminescence-excitation spectroscopy was performed using a SuperK Extreme supercontinuum laser, as previously described. Briefly, a supercontinuum laser source, operated in 3 nm steps from 500 to 839 nm, was fed through fiber optics into a $20\times$ infrared air objective (Olympus LCPLN20XIR) under an inverted microscope (Olympus IX-71). Emission was collected from 930 to 1368 nm with an Isoplane spectrometer (Princeton Instruments, resolution, 0.5 nm) and an InGaAs NIR camera (Princeton Instruments). Data were acquired with a 1 s exposure time and fit with a Lorentzian function to obtain the peak intensity and center wavelength. Photoluminescence-excitation maps were generated with MATLAB software. Experiments were conducted in $110-130~\mu$ L of total volumes containing a working mass below 250 ng (1 μ g/mL, mid-nanomolar range²⁹). The excitation fluence through each sample was approximately 0.5 J/cm².

Porphyrin Dye Fluorescence. A Tecan Infinite M1000 Pro plate reader (Tecan Group Ltd.) and UV transparent half-well 96-well plates (Corning 3679) were used to scan the fluorescence of porphyrin solutions. The following settings were used: bottom read mode, gain 255 (191 or 100 for PP without or with IGEPAL surfactant), a 500–800 nm emission window with a 5 nm bandwidth, and 2 nm step size; the following excitation wavelengths were used for 50 flashes/well at 400 Hz, 20 μ s integration, and no lag/settle (5 nm bandwidth): 370 nm for hemin, 380 nm for PP, 365 nm for IHPF, and 408 nm for MSTPF.

Statistics, Analysis, and Software. Error bars in each figure represent standard deviations derived from N=3 technical replicates. Binding/interaction affinity rank-order, derived from spectroscopic behavior, used the final maximum peak change after titration since all resulting changes were monotonic. Spectral power, detector nonlinearity, and background correction were performed on all data using MATLAB (R2014a). All emission/absorption peaks representing various SWCNT diameters were fit with a Lorentzian function without deconvolution. Reported spectra represent fits where $r^2 \geq 0.90$. OriginPro 9 was used to plot data. Adobe Illustrator CS6 was used to generate figures and diagrams. ChemBioDraw Ultra 13.0 was used to generate chemical structures. Fold change was calculated as (final/initial) -1.

RESULTS

Effect of Free and Sequestered Hemin on Coated SWCNT Spectral Properties. To assess the suitability of SWCNTs as a probe of direct and indirect porphyrin binding, we screened a library of SWCNT coatings for those capable of promoting a SWCNT emission red-shift to both free and

www.acsami.org

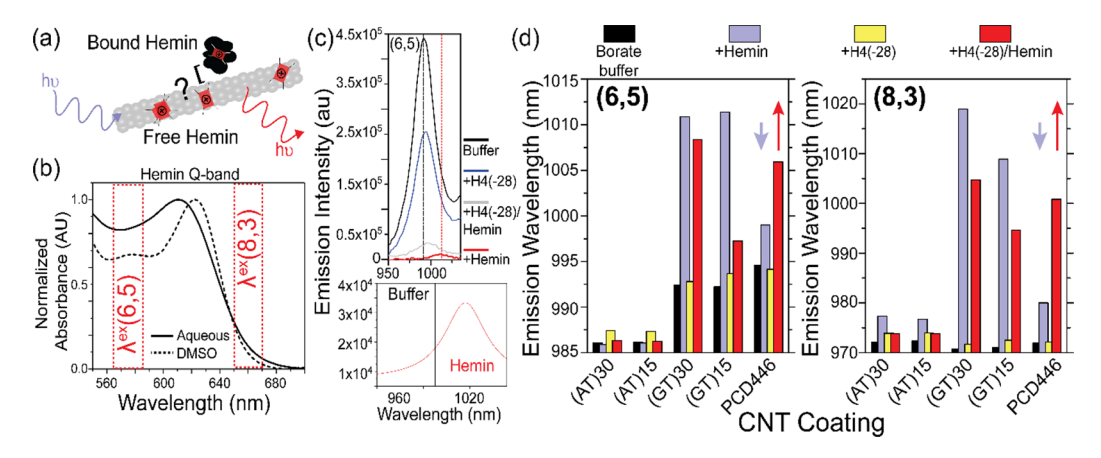


Figure 1. Chromatic red-shifts induced by free and protein-sequestered hemin. (a) Model of dye binding to an excited-state SWCNT sidewall. The dye (or dye aggregate) binds either directly to the SWCNT, or it is sequestered from the SWCNT by the protein. The coating is not shown. (b) Laser excitation profile of the SWCNT species and interacting hemin in solutions that solubilize (DMSO) or aggregate (aqueous) the porphyrin. (c) Representative spectroscopic assay of the (GT)₁₅-coated SWCNT titrated with hemin with or without binding protein. λ ex: 575 nm, 1 μ M each of hemin/protein. Vertical lines are the fit center wavelengths. The lower panel is a magnified view. (d) Fit center wavelengths from emission spectra, as in panel (c), as a function of the coating identity and SWCNT chirality. Arrows reference the text. For the entire library screen, see Figure S2. Reported data have fit $r^2 \ge 0.90$. (AT)_n/(GT)_n, ssDNA polymer of *n*-repeats; PCD, polycarbodiimide; H4(-28), hemin binding proteins.

protein-bound ferric hemin. A designed hemin binding protein, H4(-28), with a net charge count (acidic minus basic residues) of -28, was used to sequester the hemin from direct contact with the SWCNT. The coating panel consisted of (A)- or (G)-rich ssDNA, surfactants (SDC or PEG-cera), cellulose (CMC), and in-house synthesized polycarbodiimide (PCD) polymers (Figure S1). The PCD polymers contain a nitrogen-rich guanidinium backbone with phenyl and triazole groups in their side chains.

We used the screen to ask whether these coatings induce a red-shift of the SWCNT photoluminescence in response to free hemin or hemin shielded from direct contact by a binding protein and whether the coatings induce a red-shift independent of hemin excitation (Figure 1a,b). A representative subset of data from the screen is presented in Figure 1c, which shows the spectra from continuous wave laser excitation-emission of the visible S22 transition of small diameter, (6,5) and (8,3), coated SWCNTs suspended in aqueous buffer and exposed to free hemin or hemin complexed with binding protein (1:1 mole ratio). As Figure 1c shows, SWCNT fluorescence notably quenches in the presence of hemin, H4(-28) alone, or the porphyrin-bound protein complex. Among the coatings used, ssDNA rich in guanine (G) is a positive control for binding whereas ssDNA rich in adenine (A) serves as a negative control. Selected emission data from the screen of both the (6,5) and (8,3) nanotubes are depicted in Figure 1d, and data for additional coatings are depicted in Figure S2. Overall, large red-shifts from the SWCNT result from the addition of hemin alone; importantly, the guanine (G)-containing ssDNA sequences, but not adenine (A)-containing sequences, produced large SWCNT red-shifts in the presence of hemin and hemin/H4(-28). The SWCNT red-shift produced by hemin alone was often greater than the SWCNT red-shift produced by hemin/H4(-28). Interestingly, one polycarbodiimide wrapping of the nanotube, PCD-446, facilitated a hemin-binding-induced SWCNT red-shift that was greater than the SWCNT red-shift in the presence of hemin or protein alone. As Figure 1 and Figure S2 indicate, the relative emission shifts of the SWCNT acceptors did not depend significantly on SWCNT chirality since on- or off-resonance

excitation of the hemin Q-band generated similar SWCNT chromatic responses.

Testing Sidewall Binding Assumptions Using SWCNT Excitation-Emission. Due to the counter-intuitive red-shift response of the nanotube coated with polymer 446 (Figure S1) when in contact with protein-bound hemin, we further studied this coating as an exception to the rule that large red- and blueshifts result from strong π - π interactions between conjugated systems. To test this hypothesis, we asked whether polymer-SWCNT complexes titrated with a panel of porphyrins in the absence of protein (Figure S3) would produce a similar response by using a library of porphyrins in either a solventsolubilized or insoluble formats to assess porphyrin-aggregate effects (Figure S4a,b). Photoluminescence-excitation mapping was performed on 446-SWCNT, wherein excitation was scanned from 500 to 700 nm (Figure 2a). Spectroscopy was repeated by titrating each porphyrin species over a wide concentration range into solutions containing a constant mass of dissolved 446-SWCNT. Figure 2b shows the trend between porphyrin concentration and 446-SWCNT emission shift for (8,3) and (6,5) chiralities in aqueous (left column) or DMSO (right column) solvents. The red-shifted SWCNT emission was dose-dependent on hemin, PP, and IHPF dissolved in aqueous buffer. No significant red-shift was observed when porphyrins were totally solubilized in DMSO. Based on the relationship between the bathochromic shift and intermolecular interactions, we depict the affinities of the porphyrins for the polymer-nanotube complexes in Figure 2c.

Several conclusions can be drawn from these results: first, only aggregation of suspended, ionized porphyrin species produces the red-shifting response as MSTPF, a highly aqueous soluble porphyrin, exhibits no effect on emission shift. Second, two SWCNT chiralities were analyzed; one on and one off-resonance with the porphyrin Q-bands. The use of this system allowed us to discount a possible excited porphyrin-origin for the observed acceptor-SWCNT red-shift. In contrast, porphyrin titration data from the DMSO experiment did not support a concentration-dependent surface binding model for freely soluble dye interacting with the polymer-nanotube. To exclude ionic strength-related rear-

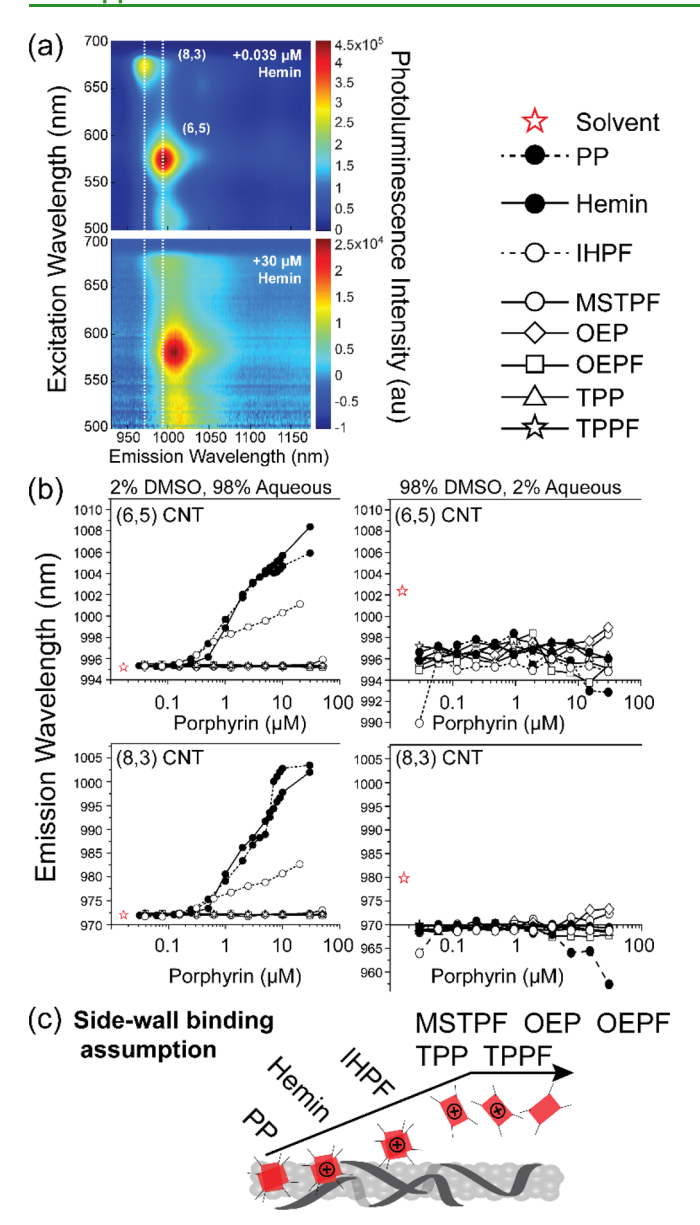


Figure 2. Initial assumption for SWCNT-porphyrin sidewall binding. (a) Representative photoluminescence excitation/emission maps of 446-SWCNT complexes upon introduction of a low (top) or high (bottom) hemin concentration. (b) Emission center wavelength of 446-SWCNT complexes as a function of porphyrin concentration for the (6,5) (top row) or (8,3) (bottom row) SWCNT species. The assay sample solvent was either aqueous buffer (left column) or nearneat DMSO (right column). (c) Empirical rank-order model of porphyrin binding on the SWCNT-coating complex. Full names of each porphyrin abbreviation are in the Experimental Section, while structures are depicted in Figure S3.

rangements of the coating polymer³⁰ or surface screening effects from the electrolyte,³¹ aqueous buffer salt components were titrated individually. Electrolyte-mediated chromatic shifts were absent (Figure S4c), indicating that the acceptor complex (coating plus nanotube; Figure S5) excited state responds solely to the porphyrin complexes.

A prior work on ssDNA-nanotube interactions with photoactive dyes relied on porphyrin donor excitation to infer interactions;⁸ this type of interaction was reasonable given the known chemical activity between DNA and porphyrin. Similarly, to rule out any cross-reactivity between

the 446 polymer coating and porphyrins, in the SWCNT, we tested each representative porphyrin from our acceptor titration screen against 446 using an ABTS enhancer-based radical assay to detect chemical interaction (charge transfer catalysis) (Figure S6). Results showing a lack of change in ABTS radical absorbance between suspended porphyrin and suspended porphyrin-polymer complexes excluded the idea that the selection of the 446 polymer under investigation was just another intrinsically strong-interacting intermediate layer on the SWCNT.

Interaction Order from Porphyrin Soret Absorption/ Emission. We next determined whether directly probing the porphyrins with light would result in similar photophysical behavior in polymer or polymer-SWCNT complexes: we titrated a constant concentration of representative porphyrins with increasing concentrations of 446 or 446-SWCNT (Figure 3a). A similar experiment was performed for each representa-

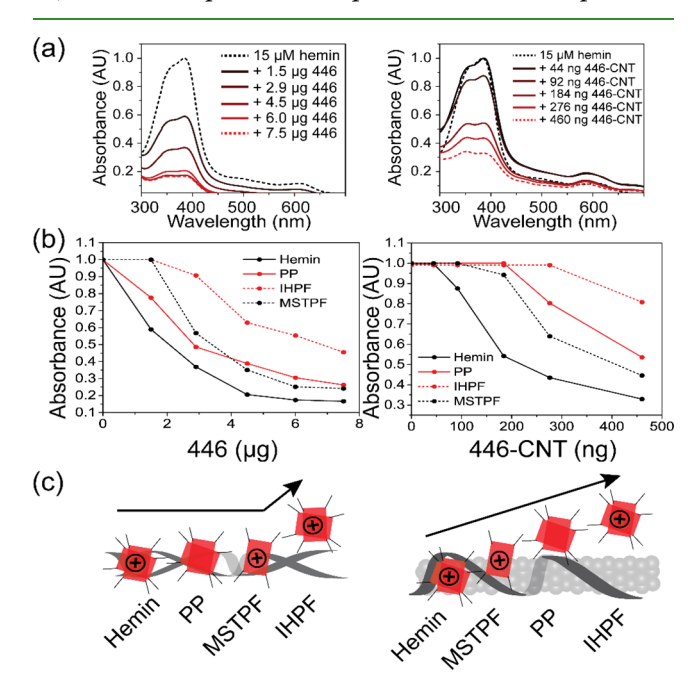


Figure 3. SWCNT-porphyrin binding assessed through the porphyrin ground state. (a) Representative raw spectra of 15 μ M hemin titrated with increasing 446 (left) or 446-CNT (right). (b) Porphyrin Soret peak absorbance as a function of the added 446 polymer or 446-SWCNT complex (reported as total mass) in aqueous buffer, in the presence of 15 μ M porphyrin. Additional raw spectra can be found in Figure S7. (c) Empirical rank-order model of porphyrin binding to the 446 coating (left) or 446-SWCNT complex (right).

tive porphyrin species, and the resulting Soret spectra peak maxima were determined. Figure 3b reports the bleaching of hemin Soret peak absorbance (Figure S7 for other species). Based on the rate of Soret bleaching in the presence of polymer or polymer-nanotube, we determined a new interaction rank-order (Figure 3c), demonstrating that the strongest porphyrin interactions with the polymer also hold for the polymer-nanotube complexes. A roughly similar trend between the polymer coating and polymer-nanotube complexes suggested that, similar to the (G)-rich ssDNA study, spectroscopy of the donor porphyrin results in a general agreement between the interaction with polymer or polymernanotube complexes, suggesting significant binding affinity with the nanotube itself. Importantly, the interaction strength

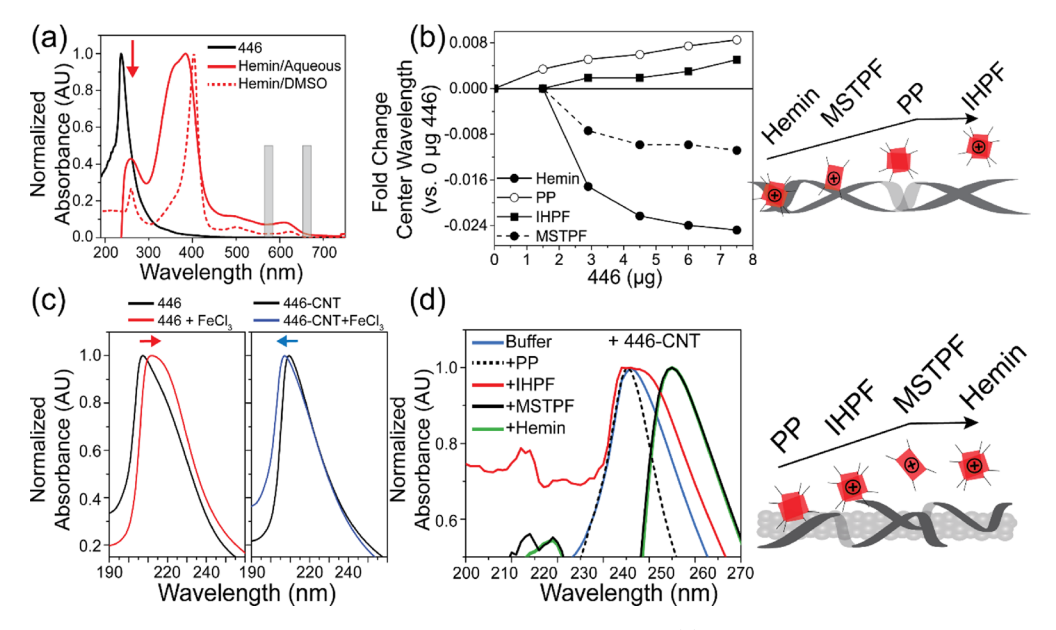


Figure 4. SWCNT-porphyrin binding assessed through UV absorbance of complexes. (a) UV-vis absorbance spectra of soluble or aggregated hemin $(1 \mu M)$ overlaid on the polymer 446 $(1 \mu M)$ spectrum. The arrow indicates an overlap. Vertical bars refer to the nanotube excitation lasers. (b) Fold change in the fit center wavelength of the main UV absorption peak (see Figure S8) before and after titration of polymer 446 with 15 μM porphyrin. An interaction rank-order from the data is depicted on the right. (c) Representative effect of aqueous iron(III) chloride salt (10 nM) on the UV absorbance of polymer 446 (left) or 446-SWCNT (right). The iron salt was used to blank. (d) Raw spectra overlay of UV absorbance peaks acquired after 92 ng of 446-SWCNT was added into buffer with or without 15 μM porphyrin. An interaction rank-order from the data is depicted on the right.

of porphyrins with polymer-nanotube complexes measured through porphyrin spectroscopy does not follow the same trend as the interaction generated by the SWCNT (acceptor) optical response.

Interaction Monitored Using Total Complex Ultraviolet (UV) Absorption. Unlike the catalytic porphyrin interaction with ssDNA-nanotube complexes,9 polymer 446 shows no such activity. To ask whether the donor and acceptor trends were mutually exclusive, we used UV absorbance as a separate assay since the porphyrin and the polymer coating overlap in the UV spectral region (Figure 4a). We surmised that UV absorbance could help to assess interactions within the whole complex via the measurements of general spectral shift and bleaching/quenching. First, we repeated a titration of the polymer alone with each representative porphyrin. Figure 4b shows the effect of the polymer titration on porphyrincoating complex absorption in the UV region as a fold change of peak shift relative to porphyrin (Figure S8a). Based on the magnitude of the UV band shifting with respect to porphyrin (horizontal line), we generated an interaction rank-order in

Next, we sought to describe the UV absorbance of the polymer-nanotube-porphyrin complex; therefore, we employed an iron ion assay to ask whether we could differentiate the SWCNT sidewall plasmon²² from the rest of the interface components. Using the same experimental conditions, we added 1 nM iron(III) chloride salt to polymer or polymernanotube complexes. Figure 4c reports representative changes to UV absorption energy after the addition of the iron ion. We observed a unique response, a hypsochromic (blue, right panel) shift for iron in the presence of polymer-nanotube complexes. When the polymer alone was in the presence of iron, we observed a bathochromic (red, left panel) shift. Furthermore, mild hypochromism of the polymer-nanotube-iron complexes (Figure S8b) confirmed that the iron ion was

interacting with the sidewall plasmon. With this optical benchmark in hand, we addressed the interaction affinity of the porphyrins with polymer-nanotube complexes. A single concentration of polymer-nanotube complexes was mixed with representative porphyrins followed by UV absorption spectrophotometry. As shown in Figure 4d, we observed a large red-shift from the hemin and MSTPF complexes. The spectra from samples containing PP and IHPF complexes, however, did not show any center of mass shift relative to polymernanotube only; rather, their peak's spectral weight (width) changed. The PP complexes lost absorbance in the Q-band region, while the IHPF sample absorbance was broadened. Using these results, we generated a third interaction rank-order in Figure 4d. By comparing each interaction rank-order for general agreement, we found that only the polymer coating was consistent throughout. Polymer-nanotube complex rank-orders did not agree. Therefore, we formulated a new molecular interface interaction model (Figure 5) to explain the discrepancy.

DISCUSSION

Here, we demonstrated that SWCNT donor—acceptor properties are strongly affected by the intervening coating and how they mediate the donor—nanotube interaction. Previous models ascribe the effects of SWCNT coating/wrappings to electronic hybridization with the carbon sidewall.^{3,5,32} One important implication of this hybridization phenomenon is that photosensitized donor—acceptor systems, which depend on how and where donors and acceptors make contact, are susceptible to inefficiencies that arise from controllable variables such as preparation, dispersion, and encapsulation. We used the polymer-nanotube-porphyrin complex as a model nanoscale interface since emission intensity changes have been observed for other aromatic chromophores that directly coat the SWCNT sidewall.³³ The coating both covers the SWCNT

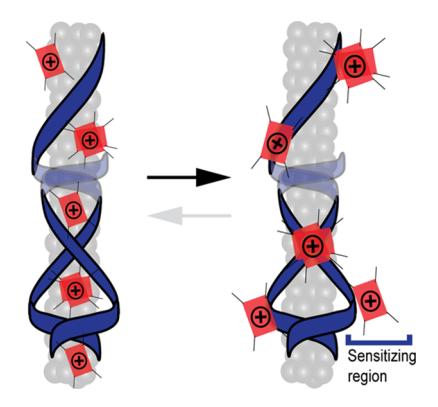


Figure 5. Proposed interfacial interaction of encapsulated-SWCNT with porphyrins. Optical evaluation of dye binding to the acceptor CNT, and non-covalent coating is not consistent with spectral methods that assume only direct interactions occur between the dye and semiconductor. The coating sensitizing region is important when spectroscopic assays attempt to probe the whole complex or parts of the complex.

sidewall and stabilizes the material in colloid. Furthermore, the coating may also interact with SWCNT excitations. In this study, we began by asking whether the acceptor complex emission response (red-shift/quench) was necessary and sufficient to infer a sidewall interaction. Several key pieces of information were gleaned from the initial spectroscopic screen using free porphyrin and protein-bound porphyrin. First, the anionic polymeric coating on SWCNTs promotes the SWCNT red-shift. Since the aqueous buffer pH was alkaline, ensuring complete ionization of porphyrin and coatings, all interactions should be repulsive. This suggests that the excited-state acceptor complex does interact strongly with the porphyrin π - π system. Furthermore, a significant SWCNT red-shift was found for self-associating yet suspended porphyrins regardless of whether porphyrin was excited at the Q-bands. Because Qband excitation probes electronic coupling of the flat porphyrin molecule parallel to an acceptor interface, 34,35 nanotube spectral shifts were likely not due to significant direct interactions with porphyrin. To corroborate this weak interaction, we used a neutral surfactant displacement assay^{6,31,36} to ask whether exposing the SWCNT sidewall would assist in porphyrin binding and porphyrin emission quenching. By adding IGEPAL CA-630 into suspension with PP (Figure S9), we found the opposite: large brightening of PP fluorescence. Importantly, porphyrins (and polymer-SWCNT) completely solubilized by DMSO had a negligible impact on acceptor emission over the titration range, with some exceptions.

By testing a library of porphyrins, an empirical non-covalent CNT-porphyrin interaction model was generated and subsequently tested using an established approach to probe porphyrin Soret optical properties⁸ as well as two approaches to probe the polymer-nanotube complex and nanotube sidewall plasmon.²² These orthogonal methods reveal that the polymer interacted with representative porphyrin species similarly. However, by comparing the initial polymer-nanotube rank-order with the rank-order produced using the Soret and UV assays, we found no compelling agreement between methods.

Few studies directly suggest that suspended polymernanotube complexes may interact with solutes through sidewall-indirect interactions. $^{4-6}$ Non-covalent interaction

studies with the SWCNT generally discuss interactions with the sidewall as a result of coating coverage changes and/or solvent dielectric changes, without mentioning the possibility that coating-intrinsic properties may contribute to optical and physical changes. The possibility of a photonic and/or chemical interaction with the coating layer was directly proposed by evidence that identified nanotube-coating hybridization.^{3,32} Our data points to a modified donor-acceptor picture based on a basic metrological (assay) caveat: spectroscopic techniques, which excite either the semiconducting SWCNT acceptor alone, the donor dye alone, or the full complex, may probe different underlying phenomena. However, due to the close contact and excitable interaction between the non-covalent coating and SWCNT, routine spectroscopy might not be able to discount the coating's impact. Our interpretation follows from a disconnect between nanotube interaction rank-orders and agrees with mounting evidence for electronic hybridization between the SWCNT excited states and the SWCNT coating layer.3,32 Molecular hybridization, while functionally important, may prove to be a concern since donor dye excitation often leads to crossexcitation of the broadly absorbing SWCNT semiconductor. Non-spectroscopic assays might not agree with spectroscopic assays where molecular interactions are correlated with application end-points, even though the former should predict the latter. Therefore, detailed investigations into the SWCNT photoexcitation process as well as the role of coating-intrinsic physicochemical properties (e.g., charge distribution during excitation) will be needed to connect spectroscopic signatures to these properties.

CONCLUSIONS

In this work, we tested a common assumption whereby donor dye binding to non-covalently coated nanotube complexes is coating-independent. By studying the excited semiconducting acceptor, we confirmed that porphyrin dye-binding (G)-rich ssDNA coatings mediated the acceptor red-shift and that this shift was attenuated by protein sequestration. However, we identified a coated nanotube complex that red-shifted in the presence of sequestered porphyrin. The importance of coatingrelated interactions on spectroscopic behavior was determined through optical excitation of the acceptor complex, the donor, or the entire donor-acceptor complex. Each method independently determined dye binding affinity with these components. Together, our results do not support affinity with the full semiconductor complex but rather the coating alone. Data supports an alternative spectroscopic picture wherein non-covalent sensitizer interactions are better described as coating-centric. Furthermore, this work supports evidence of hybridization between the semiconductor and coating that can convolute optical assessment in the absence of more complex physical imaging techniques. For example, cross-excitation of the acceptor may lead to different interpretations. Results suggest that coating-intrinsic properties, such as redox, pH, and electrostatics, will be important variables in application development.

ASSOCIATED CONTENT

Supporting Information

The Supporting Information is available free of charge at https://pubs.acs.org/doi/10.1021/acsami.1c14266.

Additional experimental figures, spectroscopic behavior, and identity of all screened coatings (PDF)

AUTHOR INFORMATION

Corresponding Author

Daniel A. Heller – Weill Cornell Medicine, Cornell University, New York, New York 10065, United States; Memorial Sloan Kettering Cancer Center, New York, New York 10065, United States; orcid.org/0000-0002-6866-0000; Email: hellerd@mskcc.org

Authors

Christopher P. Horoszko – Weill Cornell Medicine, Cornell University, New York, New York 10065, United States; Memorial Sloan Kettering Cancer Center, New York, New York 10065, United States; orcid.org/0000-0003-2344-4707

Peter J. Schnatz – Department of Physics, City College of New York, New York, New York 10031, United States

Januka Budhathoki-Uprety — Department of Textile Engineering, Chemistry and Science, North Carolina State University, Raleigh, North Carolina 27606, United States; orcid.org/0000-0003-3395-4823

Rahul V. Rao-Pothuraju — College of Arts and Sciences, New York University, New York, New York 10003, United States Ronald L. Koder — Department of Physics, City College of New York, New York, New York 10031, United States; Graduate Programs of Physics, Chemistry, Biochemistry and Biology, The Graduate Center of CUNY, New York, New York 10016, United States

Complete contact information is available at: https://pubs.acs.org/10.1021/acsami.1c14266

Author Contributions

All authors contributed to the final manuscript and approved of the final version.

Notes

The authors declare the following competing financial interest(s): D.A.H. is a cofounder and officer with equity interest in LipidSense, Inc., a cofounder and officer with equity interest in Goldilocks Therapeutics, Inc., a cofounder and officer with equity interest in Nirova Biosense, Inc., and a member of the scientific advisory board of Concarlo Holdings LLC, and Nanorobotics, Inc.

■ ACKNOWLEDGMENTS

This work was supported in part by the National Science Foundation CAREER Award (1752506), the NIH New Innovator Award (DP2-HD075698), the Cancer Center Support Grant (P30 CA008748), the Pershing Square Sohn Cancer Research Alliance, the Honorable Tina Brozman Foundation for Ovarian Cancer Research, the Expect Miracles Foundation Financial Services Against Cancer, the Anna Fuller Fund, the Louis V. Gerstner Jr. Young Investigator's Fund, the Frank A. Howard Scholars Program, MSK's Cycle for Survival's Equinox Innovation Award in Rare Cancers, the Alan and Sandra Gerry Metastasis Research Initiative, Mr. William H. Goodwin and Mrs. Alice Goodwin and the Commonwealth Foundation for Cancer Research, the Experimental Therapeutics Center, the Imaging & Radiation Sciences Program, and the Center for Molecular Imaging and Nanotechnology of Memorial Sloan Kettering Cancer Center.

C.P.H. was supported in part by the National Cancer Institute (NCI) grant NIH T32CA062948. J.B.-U. was supported in part by the Tow Foundation postdoctoral fellowship, Center for Molecular Imaging and Nanotechnology at MSKCC. R.L.K. acknowledges funding from NIH-GM111932. R.V.R.-P. was supported in part by the 2018 NYU Dean's Undergraduate Research Fund.

REFERENCES

- (1) White, C. T.; Todorov, T. N. Carbon nanotubes as long ballistic conductors. *Nature* **1998**, 393, 240–242.
- (2) Soavi, G.; Scotognella, F.; Lanzani, G.; Cerullo, G. Ultrafast Photophysics of Single-Walled Carbon Nanotubes. *Adv. Opt. Mater.* **2016**, *4*, 1670–1688.
- (3) Kahmann, S.; Salazar Rios, J. M.; Zink, M.; Allard, S.; Scherf, U.; dos Santos, M. C.; Brabec, C. J.; Loi, M. A. Excited-State Interaction of Semiconducting Single-Walled Carbon Nanotubes with Their Wrapping Polymers. *J. Phys. Chem. Lett.* **2017**, *8*, 5666–5672.
- (4) Polo, E.; Kruss, S. Impact of Redox-Active Molecules on the Fluorescence of Polymer-Wrapped Carbon Nanotubes. *J. Phys. Chem.* C 2016, 120, 3061–3070.
- (5) Horoszko, C. P.; Jena, P. V.; Roxbury, D.; Rotkin, S. V.; Heller, D. A. Optical Voltammetry of Polymer-Encapsulated Single-Walled Carbon Nanotubes. *J. Phys. Chem. C* **2019**, *123*, 24200–24208.
- (6) Jena, P. V.; Safaee, M. M.; Heller, D. A.; Roxbury, D. DNA-Carbon Nanotube Complexation Affinity and Photoluminescence Modulation Are Independent. *ACS Appl. Mater. Interfaces* **2017**, *9*, 21397–21405.
- (7) Bouanis, F. Z.; Bensifia, M.; Florea, I.; Mahouche-chergui, S.; Carbonnier, B.; Grande, D.; Léonard, C.; Yassar, A.; Pribat, D. Noncovalent functionalization of single walled carbon nanotubes with Fe-/Co-porphyrin and Co-phthalocyanine for field-effect transistor applications. *Org. Electron.* **2021**, *96*, 106212.
- (8) Zhang, H.; Bork, M. A.; Riedy, K. J.; McMillin, D. R.; Choi, J. H. Understanding Photophysical Interactions of Semiconducting Carbon Nanotubes with Porphyrin Chromophores. *J. Phys. Chem. C* **2014**, *118*, 11612–11619.
- (9) Travascio, P.; Li, Y.; Sen, D. DNA-enhanced peroxidase activity of a DNA-aptamer-hemin complex. *Chem. Biol.* **1998**, *5*, 505–517.
- (10) Scholes, G. D.; Rumbles, G. Excitons in nanoscale systems. *Nat. Mater.* **2006**, *5*, 683–696.
- (11) Zhong, Q.; Diev, V. V.; Roberts, S. T.; Antunez, P. D.; Brutchey, R. L.; Bradforth, S. E.; Thompson, M. E. Fused Porphyrin—Single-Walled Carbon Nanotube Hybrids: Efficient Formation and Photophysical Characterization. *ACS Nano* **2013**, *7*, 3466—3475.
- (12) Sprafke, J. K.; Stranks, S. D.; Warner, J. H.; Nicholas, R. J.; Anderson, H. L. Noncovalent Binding of Carbon Nanotubes by Porphyrin Oligomers. *Angew. Chem., Int. Ed.* **2011**, *50*, 2313–2316.
- (13) Cheng, F.; Adronov, A. Noncovalent Functionalization and Solubilization of Carbon Nanotubes by Using a Conjugated Zn–Porphyrin Polymer. *Chem. Eur. J.* **2006**, *12*, 5053–5059.
- (14) Redmond, R. W. Enhancement of the sensitivity of radiative and non-radiative detection techniques in the study of photosensitization by water soluble sensitizers using a reverse micelle systems. *Photochem. Photobiol.* **1991**, *54*, 547–556.
- (15) D'Souza, F.; Das, S. K.; Zandler, M. E.; Sandanayaka, A. S. D.; Ito, O. Bionano Donor–Acceptor Hybrids of Porphyrin, ssDNA, and Semiconductive Single-Wall Carbon Nanotubes for Electron Transfer via Porphyrin Excitation. *J. Am. Chem. Soc.* **2011**, *133*, 19922–19930.
- (16) Maligaspe, E.; Sandanayaka, A. S. D.; Hasobe, T.; Ito, O.; D'Souza, F. Sensitive Efficiency of Photoinduced Electron Transfer to Band Gaps of Semiconductive Single-Walled Carbon Nanotubes with Supramolecularly Attached Zinc Porphyrin Bearing Pyrene Glues. J. Am. Chem. Soc. 2010, 132, 8158–8164.
- (17) Ní Mhuircheartaigh, É. M.; Giordani, S.; Blau, W. J. Linear and Nonlinear Optical Characterization of a Tetraphenylporphyrin—Carbon Nanotube Composite System. *J. Phys. Chem. B* **2006**, *110*, 23136–23141.

- (18) Kauffman, D. R.; Kuzmych, O.; Star, A. Interactions between Single-Walled Carbon Nanotubes and Tetraphenyl Metalloporphyrins: Correlation between Spectroscopic and FET Measurements. *J. Phys. Chem. C* **2007**, *111*, 3539–3543.
- (19) Malic, E.; Weber, C.; Richter, M.; Atalla, V.; Klamroth, T.; Saalfrank, P.; Reich, S.; Knorr, A. Microscopic Model of the Optical Absorption of Carbon Nanotubes Functionalized with Molecular Spiropyran Photoswitches. *Phys. Rev. Lett.* **2011**, *106*, No. 097401.
- (20) Malic, E.; Setaro, A.; Bluemmel, P.; Sanz-Navarro, C. F.; Ordejon, P.; Reich, S.; Knorr, A. Carbon nanotubes as substrates for molecular spiropyran-based switches. *J. Phys.: Condens. Matter* **2012**, 24, 394006.
- (21) Kreft, S. K.; Petersen, M. Å.; Nielsen, M. B.; Reich, S.; Setaro, A. Isomerization of Orthogonal Molecular Switches Encapsulated within Micelles Solubilizing Carbon Nanotubes. *J. Phys. Chem. C* **2015**, *119*, 15731–15734.
- (22) Cheung, W.; Patel, M.; Ma, Y.; Chen, Y.; Xie, Q.; Lockard, J. V.; Gao, Y.; He, H. π -Plasmon absorption of carbon nanotubes for the selective and sensitive detection of Fe3+ ions. *Chem. Sci.* **2016**, 7, 5192–5199.
- (23) Gu, Z.; Yang, Z.; Chong, Y.; Ge, C.; Weber, J. K.; Bell, D. R.; Zhou, R. Surface Curvature Relation to Protein Adsorption for Carbon-based Nanomaterials. *Sci. Rep.* **2015**, *5*, 10886.
- (24) Yu, G.; Zhou, J. Understanding the curvature effect of silica nanoparticles on lysozyme adsorption orientation and conformation: a mesoscopic coarse-grained simulation study. *Phys. Chem. Chem. Phys.* **2016**, *18*, 23500–23507.
- (25) Budhathoki-Uprety, J.; Jena, P. V.; Roxbury, D.; Heller, D. A. Helical Polycarbodiimide Cloaking of Carbon Nanotubes Enables Inter-Nanotube Exciton Energy Transfer Modulation. *J. Am. Chem. Soc.* **2014**, *136*, 15545–15550.
- (26) Schnatz, P. J.; Brisendine, J. M.; Laing, C. C.; Everson, B. H.; French, C. A.; Molinaro, P. M.; Koder, R. L. Designing heterotropically activated allosteric conformational switches using supercharging. *Proc. Natl. Acad. Sci. U. S. A.* **2020**, *117*, 5291–5297.
- (27) Zhang, L.; Andersen, E. M. E.; Khajo, A.; Maggliozzo, R. S.; Koder, R. L. Dynamic factors affecting gaseous ligand binding in an artificial oxygen transport protein. *Biochemistry* **2013**, *52*, 447–455.
- (28) Zhang, L.; Anderson, J. L.; Ahmed, I.; Norman, J. A.; Negron, C.; Mutter, A. C.; Dutton, P. L.; Koder, R. L. Manipulating cofactor binding thermodynamics in an artificial oxygen transport protein. *Biochemistry* **2011**, *50*, 10254–10261.
- (29) Galassi, T. V.; Jena, P. V.; Roxbury, D.; Heller, D. A. Single Nanotube Spectral Imaging To Determine Molar Concentrations of Isolated Carbon Nanotube Species. *Anal. Chem.* **2017**, *89*, 1073–1077.
- (30) Salem, D. P.; Gong, X.; Liu, A. T.; Koman, V. B.; Dong, J.; Strano, M. S. Ionic Strength-Mediated Phase Transitions of Surface-Adsorbed DNA on Single-Walled Carbon Nanotubes. *J. Am. Chem. Soc.* **2017**, *139*, 16791–16802.
- (31) Harvey, J. D.; Zerze, G. H.; Tully, K. M.; Mittal, J.; Heller, D. A. Electrostatic Screening Modulates Analyte Binding and Emission of Carbon Nanotubes. *J. Phys. Chem. C* **2018**, *122*, 10592–10599.
- (32) Milko, M.; Puschnig, P.; Blondeau, P.; Menna, E.; Gao, J.; Loi, M. A.; Draxl, C. Evidence of Hybrid Excitons in Weakly Interacting Nanopeapods. *J. Phys. Chem. Lett.* **2013**, *4*, 2664–2667.
- (33) Ehli, C.; Rahman, G. M. A.; Jux, N.; Balbinot, D.; Guldi, D. M.; Paolucci, F.; Marcaccio, M.; Paolucci, D.; Melle-Franco, M.; Zerbetto, F.; Campidelli, S.; Prato, M. Interactions in Single Wall Carbon Nanotubes/Pyrene/Porphyrin Nanohybrids. *J. Am. Chem. Soc.* **2006**, 128, 11222–11231.
- (34) Scolaro, L. M.; Castriciano, M.; Romeo, A.; Patanè, S.; Cefalì, E.; Allegrini, M. Aggregation Behavior of Protoporphyrin IX in Aqueous Solutions: Clear Evidence of Vesicle Formation. *J. Phys. Chem. B* **2002**, *106*, 2453–2459.
- (35) Siggel, U.; Bindig, U.; Endisch, C.; Komatsu, T.; Tsuchida, E.; Voigt, J.; Fuhrhop, J.-H. Photophysical and photochemical properties of porphyrin aggregates. *Ber. Bunsengesellschaft Phys. Chem.* **1996**, *100*, 2070–2075.

(36) Harvey, J. D.; Jena, P. V.; Baker, H. A.; Zerze, G. H.; Williams, R. M.; Galassi, T. V.; Roxbury, D.; Mittal, J.; Heller, D. A. A carbon nanotube reporter of microRNA hybridization events in vivo. *Nat. Biomed. Eng.* **2017**, *1*, 0041.